Symmetry-Selective Third-Harmonic Generation from Plasmonic Metacrystals

Shumei Chen,[1,2] Guixin Li,[1,2] Franziska Zeuner,[3] Wing Han Wong,[4] Edwin Yue Bun Pun,[4] Thomas Zentgraf,[3,*] Kok Wai Cheah,[2,†] and Shuang Zhang[1,‡]

[1]School of Physics & Astronomy, University of Birmingham, Birmingham B15 2TT, United Kingdom
[2]Department of Physics, Hong Kong Baptist University, Kowloon Tong, Hong Kong
[3]Department of Physics, University of Paderborn, Warburger Straße 100, D-33098 Paderborn, Germany
[4]Department of Electronic Engineering, City University of Hong Kong, 83 Tat Chee Avenue, Hong Kong

(Received 26 March 2014; revised manuscript received 2 June 2014; published 16 July 2014)

Nonlinear processes are often governed by selection rules imposed by the symmetries of the molecular configurations. The most well-known examples include the role of centrosymmetry breaking for the generation of even harmonics, and the selection rule related to the rotational symmetry in harmonic generation for fundamental beams with circular polarizations. While the role of centrosymmetry breaking in second harmonic generation has been extensively studied in plasmonic systems, the investigation of selection rules pertaining to circular polarization states of harmonic generation is limited to crystals, i.e., symmetries at the atomic level. In this Letter we demonstrate the rotational symmetry dependent third harmonic generation from nonlinear plasmonic metacrystals. We show that the selection rule can be imposed by the rotational symmetry of metacrystals embedded into an isotropic organic nonlinear thin film. The results presented here may open new avenues for designing symmetry-dependent nonlinear optical responses with tailored plasmonic nanostructures.

DOI: 10.1103/PhysRevLett.113.033901 PACS numbers: 42.65.Ky, 78.20.-e, 78.67.Qa

In conventional nonlinear optics, the selection rules of harmonic generation and other nonlinear optical processes are mainly based on the symmetries at the most fundamental levels, such as of molecular structures and atomic crystal configurations [1,2]. However, the macroscopic symmetry of photonic crystals, nanoparticles, quantum dots, and liquid crystals may lead to new selection rules for the nonlinear optical processes. The importance of macroscopic symmetry is especially prominent in plasmonic nanostructures, in which localized surface plasmon polariton excitations can be very sensitive to shape, size, and the surrounding medium [3]. The strong field localization in plasmonic nanostructures has been utilized to enhance the second harmonic generation (SHG) [4–14], third harmonic generation (THG) [15–18], and four-wave mixing [19–21]. In the past several years, much work has been dedicated to the investigation of SHG in plasmonic structures with broken centrosymmetry, such as split ring resonators [4], coaxial gaps [5], *L*- and *V*-shaped nanorods [6,7], and *G*-type chiral metamolecules [8]. Very recently, symmetry related selection rules were investigated in chiral metamaterials with fourfold rotational symmetry. It was found that the four-wave mixing only occurs when the signal beam and the pump beam have the same circular polarization, and the resulting nonlinear generated beam has the same circular polarization as well [22].

It was discovered that harmonic generation with circularly polarized light obeys certain selection rules that relate the order of harmonic generation to the rotational symmetry of the molecules [23–25]. The selection rules state that for a circularly polarized fundamental wave propagating along the axis of a crystal or molecule with n-fold rotational symmetry, the allowed orders for harmonic generation are $m = nl \pm 1$, with l being an arbitrary integer, $n \geq 3$ representing the symmetry order, and the "+" and "−" sign corresponding to harmonic generation of the same or opposite circular polarization state, respectively. Based on the selection rules for THG, circularly polarized light cannot generate a third harmonic wave in isotropic media [23–27], since the spin angular momentum of the light would not be conserved in such processes. One interesting property of THG with circular polarization is that circularly polarized light produces THG with only opposite handedness when it propagates along the axis of a crystal with fourfold rotational symmetry [26,27]. This rule holds for the microscopic molecular symmetry; however, it has not been experimentally verified at the more macroscopic symmetry level of artificial nanostructures, where the significant enhancement of the field due to the strong interaction between light and the nanostructure greatly increases the efficiency of the nonlinear processes.

For the investigation of the correlation between rotational symmetry and third harmonic generation of circularly polarized light, we designed three types of two-dimensional plasmonic crystals consisting of an array of rectangular nanorods with $C2$ rotational symmetry, nano crosses with $C4$ symmetry, and three pedal nanorods with $C3$ symmetry [Fig. 1(a)]. The nanostructures with $C2$ and $C4$ symmetries are arranged in a square lattice, whereas structures with $C3$ symmetry are arranged in a hexagonal lattice, such that the

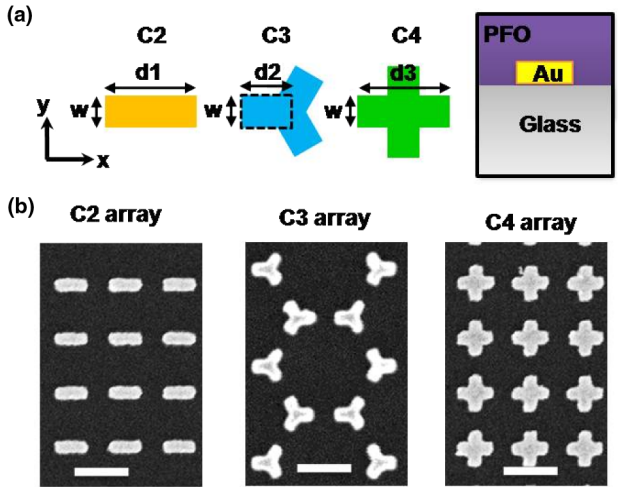

FIG. 1 (color online). Schematic of nanostructures of various rotational symmetries. (a) Geometry of plasmonic crystals with $C2$, $C3$, and $C4$ rotational symmetries. The unit cell consists of gold nanorods embedded in a thin PFO film. The width of the nanorods is $w = 50$ nm, and the lengths of the nanorods are $d_1 = 230$ nm, $d_2 = 110$ nm, and $d_3 = 210$ nm, respectively. The center to center distance between two adjacent unit elements is 400 nm with a thickness of gold structures of $t = 30$ nm. (b) Scanning electron microscopy images of the gold nanorod samples with $C2$, $C3$, and $C4$ symmetry fabricated by electron beam lithography. The scale bar represents 400 nm.

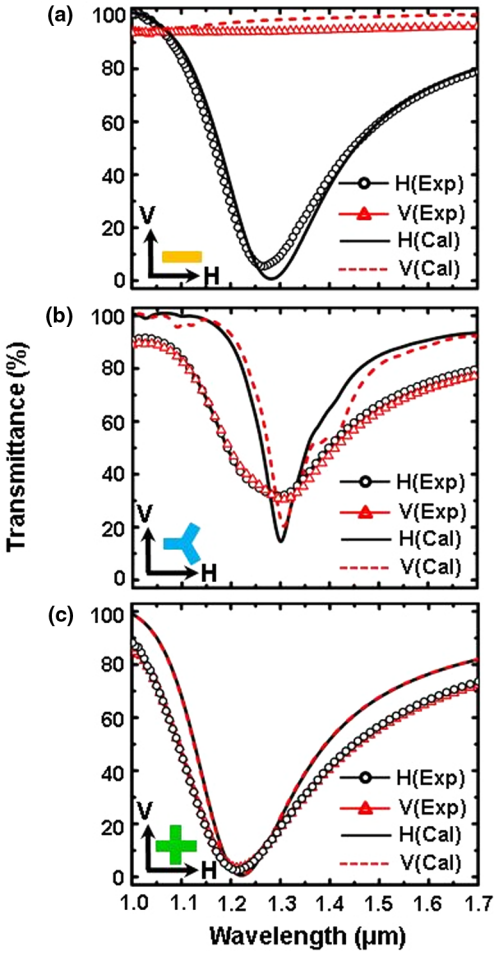

FIG. 2 (color online). Linear optical characterization of the metacrystals. Measured (solid lines with circle and triangle symbols) and calculated (solid and dashed lines) transmission spectra for the gold-PFO plasmonic hybrid crystals with $C2$ (a), $C3$ (b), and $C4$ (c) rotational symmetries. The spectra show the plasmonic resonance of the structures for illumination with horizontal (H) and vertical (V) polarized light. (See the inset for the orientation of the axes.)

symmetries of the structures and the lattice are consistent with each other. We will show later that, due to the deep subwavelength thickness of the plasmonic crystal, the selection rule can be extended to lower rotational symmetry $C2$. The gold nanostructures with $C2$, $C3$, and $C4$ symmetries were fabricated by using electron beam lithography and a metal lift-off process. The geometries of the samples are chosen such that all samples show similar plasmonic resonance wavelengths in the near-infrared spectral range. Subsequently, a 100-nm-thick poly(9,9-dioctylfluorence) (PFO) film that has a high third-order nonlinearity was coated onto the plasmonic crystals to generate the THG in the experiments. The scanning electron micrographs of the samples with the three different symmetries are shown in Fig. 1(b).

For normal light incidence the linear optical properties of the samples are characterized by measuring the polarization dependent transmission spectra using Fourier transform infrared spectrometry (Fig. 2). The transmission dips correspond to the excitation of localized surface plasmon polariton (LSPP) resonances supported by the finite geometry of the nanostructures. For the $C2$ symmetry sample, the LSPP resonance is around 1269 nm in the near infrared for illumination with horizontal (H) polarization (along the long axis of the rod), and in the visible for vertical (V) polarized illumination (perpendicular to the rod). For the $C3$ symmetry sample, the LSPP resonances are at 1250 nm (H) and 1260 nm (V). For the $C4$ symmetry sample, ideally, the LSPP resonances for H and V polarization should occur at the same wavelength. However, the measured resonance wavelengths are slightly different for the two linear polarizations (1207 nm for H polarization and 1219 nm for V polarization) due to the imperfection of fabrication processes. For all the samples, the numerically simulated spectra closely match the measurements.

The third harmonic generation measurements [Fig. 3(a)] were performed using a femtosecond-laser pumped optical parametric oscillator (repetition frequency, 80 MHz; pulse duration, ~200 fs; averaged power, $P = 8$ mW) at a wavelength of $\lambda = 1.25$ μm, which is close to the LSPP wavelength of all three plasmonic metacrystals. In the measurement, the fundamental pulses are focused to a spot with a diameter of ~50 μm using an infinity-corrected objective lens (5x, N.A. = 0.10) with a focal length of

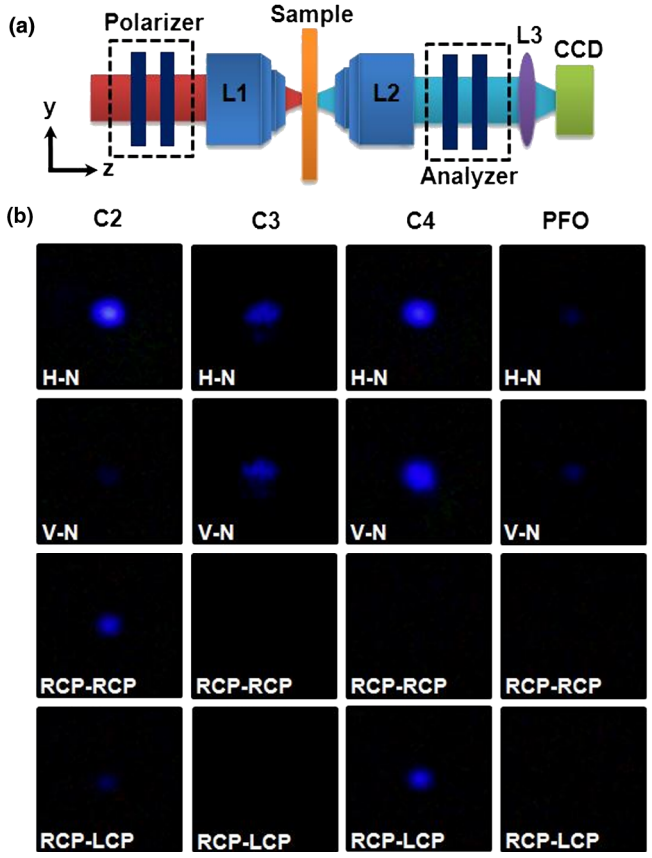

FIG. 3 (color online). Experimental results for the THG. (a) Experimental setup for the THG measurement. The polarization of the pump light was controlled by the polarizer assembly, which contains one linear polarizer and one quarter wave plate. The first objective lens ($L1$) was used to focus the light onto the plasmonic crystals. The second objective lens ($L2$) was used to collect the generated THG signals. Finally, the THG signal was imaged by a planar convex lens to a CCD camera. (b) Measured intensities of the THG signal from the samples with $C2$, $C3$, $C4$ symmetry as well as a bare PFO film for different polarization states of pump light. The first two rows show the results for pumping with linear polarization: horizontal (H) and vertical (V), receptively. "N" means that no polarizer is used for the THG signal collection. The THG signals of the third and fourth rows were recorded using right circularly polarized pump light. The third row corresponds to the right circularly polarized component of the third harmonic signal whereas the fourth row shows the left circularly polarized component.

25.8 mm. The resulting THG signal from the gold-PFO hybrid samples is collected in transmission by a second infinity-corrected objective lens (5x, N.A. = 0.10) and imaged onto a color charge coupled device (CCD) camera after filtering out the fundamental wavelength using a bandpass filter (315–710 nm).

The CCD images of the THG signal at a wavelength of 417 nm from the three samples are shown in Fig. 3(b), and the measured intensities of the THG signal are summarized in Table I. As expected, we observe a THG signal from all three samples when illuminated with linearly polarized light as no selection rule prohibits the THG for linearly polarized light. Compared to the THG from a pure PFO reference film, the LSPP resonance of the gold nanorods dramatically improves the efficiency of THG due to the near field enhancement in the vicinity of the gold nanorods. For the $C2$ symmetry metacrystal, the THG intensity for H polarization is much higher than that for V polarization. This behavior reflects the linear optical properties of the $C2$ nanorods and shows that the excitation of the vertical polarization state is nonresonant [Fig. 2(a)]. For samples with $C3$ and $C4$ symmetries, the THG for both H and V polarizations are of similar intensities as both of the two polarization states can excite the LSPP resonance at the fundamental frequency in the near infrared [Figs. 2(b) and 2(c)]. We also observe a THG signal from a surface with only gold nanorods that are not embedded into a PFO film. Our measurements show that the THG signals from the gold-PFO hybrid system are much stronger than those from both the bare gold nanorods sample and the PFO film without gold structures (see the Supplemental Material [28]). This clearly proves that the nonlinear signal is generated in the PFO film, whereas the gold nanorods mainly contribute to the field enhancement.

TABLE I. Normalized intensity of the THG measured on $C2$, $C3$, and $C4$ symmetry metacrystals. N means that no polarizer is used for THG signal collection; "$\cdots$" an empty cell means that the signal is too weak to be observed.

	$C2$	$C3$	$C4$
H-N	1	1	1
V-N	0.02	0.70	0.91
R-R	0.18	$\cdots$	0.01
R-L	0.02	$\cdots$	0.30

In the next step we carried out the THG measurements for circularly polarized light [Fig. 3(b)]. For the bare PFO film we do not observe any THG signal within our detection limit. This result agrees with the selection rules for THG; in fact the thin PFO film on the glass substrate with the organic molecules randomly oriented can be treated as an isotropic medium [22–26]. However, once the plasmonic nanorods are embedded into the PFO film, they significantly change the local field distribution and thus alter the THG process. Besides the strong field enhancement at the fundamental wavelength, as shown by the near field plot in Figs. 4(a)–4(c), the polarization state of the local electric field in the vicinity of the plasmonic structures is strongly modified by the presence of the LSPP resonance mode and is in general not circularly polarized [Figs. 4(d)–4(f)]. The local nonlinear polarization density in the isotropic polymer is given by $\vec{P}^{3\omega} = \chi^{(3)}\vec{E}(\vec{E}\cdot\vec{E})$ and its magnitude can be expressed as $|\vec{P}^{3\omega}| = \chi^{(3)}|\vec{E}|^3\delta$, where $\delta = |(\vec{E}\cdot\vec{E})|/|\vec{E}|^2$ represents the polarization state, with $\delta = 0$ for circular polarizations and

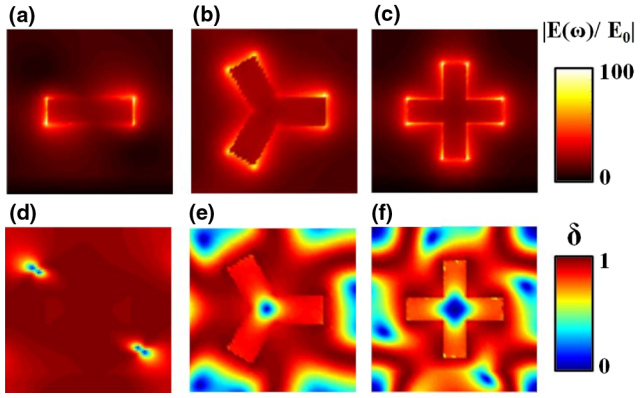

FIG. 4 (color online). Calculated field distribution in the structures with various rotational symmetries. (a)–(c) Enhancement of the electric field in the near field for the $C2$, $C3$, and $C4$ plasmonic structures. (d)–(f) The distribution of polarization state for $C2$, $C3$, and $C4$ structures, with blue color ($\delta = 0$) and red color ($\delta = 1$) denoting circular polarization and linear polarization, respectively. In all the calculations, the incident beam is right handed circularly polarized. In the regions close to the tips of the nanostructures, not only is the field enhancement very strong, but also the field is very close to linear polarization.

$\delta = 1$ for linear polarizations. As shown in Fig. 4(b), close to the tip where the field is strongly enhanced, the polarization state is close to linear polarization. This gives rise to nonzero local third-order nonlinear polarization, whose emission into the far field is further mediated by the linear response of the plasmonic structures at the THG wavelength. Interestingly, although the local third-order nonlinear polarization is nonzero, the overall THG from the $C3$ symmetry sample vanishes in the far field. This is dictated by the selection rule $m = 3l \pm 1$ for $C3$ symmetry, according to which the allowed orders of harmonic generation with the same circular polarization as the fundamental wave are $m = [1, 4, 7, \ldots]$ and those of the opposite circular polarization are $m = [2, 5, 8, \ldots]$, with $m = 3$ not present in either circular polarization state.

More intriguing results come from the comparison of the THG signals between the $C2$ and $C4$ samples. Strong optical spin dependent THG signals are observed when the circularly polarized fundamental wave is incident onto the $C2$ and $C4$ symmetry samples. For the $C2$ symmetry sample, right circularly polarized light illumination generates THG signals with both right circular polarization (RCP) and left circular polarization (LCP), as both are not forbidden by the selection rules $m = 2l \pm 1$, which allows any odd orders of harmonic generations for both circular polarizations. However, the RCP component of the THG signal is much stronger than the LCP component, with a polarization ratio between the LCP and RCP intensities of $\eta_{C2}(\mathrm{THG_{LCP}}/\mathrm{THG_{RCP}}) = 0.121$. This ratio is not governed by the selection rule, but due to the specific design of the antenna geometry. Since both LCP and RCP are allowed by the selection rule for the $C2$ symmetry, this ratio is in general not zero or infinity. However, their respective intensities can be controlled by the specific geometry of the antenna, such as the length and width of the gold rod, which determine the plasmonic resonances in both directions and the field distribution at both the fundamental and THG wavelengths. Therefore, it is expected that by adjusting the geometry of the antenna with $C2$ symmetry, the ratio between the THG signals of the two circular polarizations can be finely tailored.

Interestingly, for the $C4$ symmetry sample, the LCP component dominates in the RCP induced THG signals, with an extremely large polarization ratio η_{C4} ($\mathrm{THG_{LCP}}/\mathrm{THG_{RCP}}$) of ~29. According to the selection rule for $C4$ rotational symmetry $m = 4l \pm 1$, under illumination of a RCP fundamental wave, the allowed harmonic generations are [1, 5, 9, …] for RCP and [3, 7, 11, …] for LCP. Thus, the THG signal should be solely in the LCP state and THG of the right circularly polarized light should be forbidden; however, surface roughness and deviations of the ideal symmetry shape of the nanostructures arising from the imperfectness of nanofabrication slightly break the rotational symmetry and lead therefore to a small THG signal in the RCP state. Hence, all the experimental observations are consistent with the selection rules of THG with circularly polarized light excitation in crystal optics when generalized to 2D metacrystals with twofold rotational symmetry [27]. Indeed, the selection rules for harmonic generations in the 2D nonlinear plasmonic system can be understood through a simple coordinate rotation argument, which is presented in details in the Supplementary Material [28].

In conclusion, we have investigated the impact of rotational symmetry on the third harmonic generation for circularly polarized light in nonlinear plasmonic metacrystals. We showed that THG with a circularly polarized incident beam can only be generated in plasmonic structures with two- and fourfold rotational symmetries, but is forbidden in the threefold rotational symmetry configuration. The experimental observations of the three types of plasmonic structures exhibit selection rules that have been observed previously only at the atomic crystal or molecular levels. Our study paves the way towards the design of novel spin dependent nonlinear plasmonic devices.

This work was partly supported by EPSRC (EP/J018473/1) and NSFC (Grant No. 61328503). T. Z. and S. Z. acknowledge financial support by the European Commission under the Marie Curie Career Integration Program. F. Z. and T. Z. acknowledge financial support by the DFG Priority Program SPP1391. K. W. C. and E. Y. B. P. acknowledge support from the Research Grant Council of Hong Kong under Projects No. HKUST2/CRF/11G and No. AoE/P-02/12. G. L. thanks Donal Donat Conor Bradley for fruitful discussions on nonlinear optical materials. S. C., G. L., and F. Z. contributed equally to this work.

*thomas.zentgraf@uni-paderborn.de
†kwcheah@hkbu.edu.hk
‡s.zhang@bham.ac.uk

[1] Y. R. Shen, *The Principles of Nonlinear Optics* (John Wiley & Sons, New York, 1991).
[2] R. W. Boyd, *Nonlinear Optics* (Academic Press, San Diego, 2008).
[3] M. Kauranen and A. V. Zayats, Nat. Photonics **6**, 737 (2012).
[4] M. W. Klein, C. Enkrich, M. Wegener, and S. Linden, Science **313**, 502 (2006).
[5] W. Fan, S. Zhang, N.-C. Panoiu, A. Abdenour, S. Krishna, R. M. Osgood,, K. J. Malloy, and S. R. J. Brueck, Nano Lett. **6**, 1027 (2006).
[6] S. Kujala, B. K. Canfield, M. Kauranen, Y. Svirko, and J. Turunen, Phys. Rev. Lett. **98**, 167403 (2007).
[7] R. Czaplicki, H. Husu, R. Siikanen, J. Makitalo, and M. Kauranren, Phys. Rev. Lett. **110**, 093902 (2013).
[8] V. K. Valev, A. V. Silhanek, N. Verellen, W. Gillijns, P. Van Dorpe, O. A. Aktsipetrov, G. A. E. Vandenbosch, V. V. Moshchalkov, and T. Verbiest, Phys. Rev. Lett. **104**, 127401 (2010).
[9] V. K. Valev *et al.*, ACS Nano **5**, 91 (2011).
[10] Y. Zhang, N. K. Grady, C. Ayala-Orozco, and N. J. Halas, Nano Lett. **11**, 5519 (2011).
[11] K. D. Ko, A. Kumar, K. Hung Fung, R. Ambekar, G. Logan Liu, N. X. Fang, and K. C. Toussaint, Nano Lett. **11**, 61 (2011).
[12] W. Cai, A. P. Vasudev, and M. L. Brongersma, Science **333**, 1720 (2011).
[13] H. Aouani, M. Navarro-Cia, M. Rahmani, T. P. H. Sidiropoulos, M. Hong, R. F. Oulton, and S. A. Maier, Nano Lett. **12**, 4997 (2012).
[14] S. Linden, F. B. P. Niesler, J. Förstner, Y. Grynko, T. Meier, and M. Wegener,Phys. Rev. Lett. **109**, 015502 (2012).
[15] M. Hentschel, T. Utikal, H. Giessen, and M. Lippitz, Nano Lett. **12**, 3778 (2012).
[16] T. Utikal, T. Zentgraf, T. Paul, C. Rockstuhl, F. Lederer, M. Lippitz, and H. Giessen, Phys. Rev. Lett. **106**, 133901 (2011).
[17] T. Hanke, G. Krauss, D. Träutlein, B. Wild, R. Bratschitsch, and A. Leitenstorfer, Phys. Rev. Lett. **103**, 257404 (2009).
[18] H. Liu, G. X. Li, K. F. Li, S. M. Chen, S. N. Zhu, C. T. Chan, and K. W. Cheah, Phys. Rev. B **84**, 235437 (2011).
[19] S. M. Chen, W. H. Wong, E. Y. B. Pun, K. W. Cheah, and G. X. Li, Adv. Opt. Mater. **1**, 522 (2013).
[20] J. Renger, R. Quidant, N. Van Hulst, and L. Novotny, Phys. Rev. Lett. **104**, 046803 (2010).
[21] P. Genevet, J.-P. Tetienne, E. Gatzogiannis, R. Blanchard, M. A. Kats, M. O. Scully, and F. Capasso, Nano Lett. **10**, 4880 (2010).
[22] A. Rose, D. A. Powell, I. V. Shadrivov, D. R. Smith, and Y. S. Kivshar, Phys. Rev. B **88**, 195148 (2013).
[23] O. E. Alon, V. Averbukh, and N. Moiseyev, Phys. Rev. Lett. **80**, 3743 (1998).
[24] O. E. Alon and N. Moiseyev, Phys. Rev. A **46**, 3807 (1992).
[25] P. Zdanska, V. Averbukh, and N. Moiseyev, J. Chem. Phys. **118**, 8726 (2003).
[26] W. K. Burns and N. Bloembergen, Phys. Rev. B **4**, 3437 (1971).
[27] S. Bhagavantam and P. Chandrasekhar, Proc. Indian Acad. Sci. A **76**, 13 (1972).
[28] See Supplemental Material at http://link.aps.org/supplemental/10.1103/PhysRevLett.113.033901 for (i) comparison between third harmonic generation from the hybrid plasmonic PFO metacrystal, and those from two control samples—plasmonic metacrystal with PFO, and PFO film without plasmonic structures, (ii) detailed derivation of the selection rule of third harmonic generation from the 2D plasmonic metacrystals.